Computational Materials Science 83 (2014) 474–480

Contents lists available at ScienceDirect

Computational Materials Science

journal homepage: www.elsevier.com/locate/commatsci

Structural, elastic, thermal, electronic and optical properties of Ag_2O under pressure

Haleem Ud Din [a], A.H. Reshak [b,c,*]

[a] Department of Physics, Hazara University, KPK, Mansehra, Pakistan
[b] New Technologies – Research Center, University of West Bohemia, Univerzitni 8, 306 14 Pilsen, Czech Republic
[c] Center of Excellence Geopolymer and Green Technology, School of Material Engineering, University Malaysia Perlis, 01007 Kangar, Perlis, Malaysia

ARTICLE INFO

Article history:
Received 26 August 2013
Received in revised form 7 November 2013
Accepted 10 November 2013

Keywords:
Structural
Elastic
Thermal
Electronic
Optical properties
Under-pressure

ABSTRACT

In present paper, the structural, elastic, thermal, electronic, optical properties at ambient and high-pressure study of Ag_2O are performed using the full-potential linearized augmented plane wave (FP-LAPW) method within the framework of Density functional theory (DFT) as implemented in Wien2k Code. We have used the local density approximation (LDA), Generalized Gradient approximation (GGA) and Engel–Vosko generalized gradient approximation (EV–GGA) for calculating structural properties at 0.0–20.0 GPa pressure. The lattice constant obtained at 0.0 GPa using GGA method, is in good agreement with available experimental results. Decrease in lattice constant is observed with increase in pressure from 0.0 to 20.0 GPa. The electronic, optical and band structure calculations are also carried out using modified Becke–Johnson exchange correlation potential plus generalized gradient approximation (mBJ–GGA). At zero pressure, the calculated band gap using mBJ potential is found to be narrow, direct and comparatively better than calculated through LDA, GGA and EV–GGA. Also, the band gap increases with increase in pressure from 0.0 to 20.0 GPa. From elastic calculations, it is noted that Ag_2O is elastically stable and have ductile nature. Moreover, it is revealed that Ag_2O is suitable for optoelectronic devices.

1. Introduction

Silver oxide (Ag_2O) having direct band gap around 1.4 eV is a p-type semiconductor [1], used in optical memory [2], photography [3] and as solar energy converter [4]. It has been widely studied for its important roles in fast-ion-conducting glasses of the type AgI–Ag_2O–B_2O_3, AgI–Ag_2O–V_2O_3, and AgI–$Ag_2OP_2O_5$ [5,6]. Bond nature study between Ag and O is helpful to understand the ionic conduction mechanism and micro structure of glass [7]. Ag_2O has cuprite structure (like Cu_2O) with space group pn-3m(#224) [7]. We should emphasize that one of the main interesting properties of cuprite Ag_2O is its negative thermal expansion behavior [8,9], another noteworthy property of Ag_2O is the structural phase transition which occurs at about 35 K [10–12]. The purpose of present work is to study the structural, elastic, electronic, thermal, optical properties of Ag_2O compound at ambient and under high pressure using the full-potential linearized augmented plane wave (FP-LAPW) method.

In the present paper, a brief introduction is given in Section 1. Method of calculation is presented in Section 2 of this paper. Results and discussions are given in Section 3 and finally concluding remarks are presented in Section 4.

2. Method of calculation

In this paper, we have calculated the Structural, elastic, electronic, and optical properties of Ag_2O compound in the cuprite structure [7] at ambient and under pressure. These calculations are carried out within the framework of the density functional theory [13] using the full potential linearized augmented plane wave (FP-LAPW) [14] method, as implemented in the Wien2k Code [15]. We have used the local density approximation (LDA) [16], Generalized Gradient approximation (GGA) [17], Engel–Vosko generalized gradient approximation (EV–GGA) [18] and the modified Becke–Johnson exchange correlation potential plus Wu–Cohen version of generalized gradient approximation (mBJ–GGA). The mBJ exchange potential [19] was developed from a semi-local exchange potential proposed by Becke and Johnson (BJ-exchange potential) [20]. In the generalized gradient approximation (GGA) [17], the exchange correlation potential was treated for the self consistent calculations. Band structure calculations are carried out using LDA, GGA, EV–GGA and mBJ methods at 0–20 GPa pressure. The modified Becke–Johnson exchange potential (TB-mBJ) [19] yields very accurate electronic band structures and gaps for various types of semiconductors and insulators (e.g., sp semiconductors, noble-gas solids, and transition-metal oxides). As LDA and GGA underestimate band gaps and the electronic band dispersions, thus we will demonstrate the results obtained by mBJ–GGA–WC technique.

* Corresponding author at: New Technologies – Research Center, University of West Bohemia, Univerzitni 8, 306 14 Pilsen, Czech Republic. Tel.: +420 777 729 583.
E-mail address: maalidph@yahoo.co.uk (A.H. Reshak).

0927-0256/$ - see front matter © 2013 Elsevier B.V. All rights reserved.
http://dx.doi.org/10.1016/j.commatsci.2013.11.021

In the FP-LAPW method, the wave function, charge density and potential are expanded in spherical harmonic functions inside muffin-tin spheres and by a plane-waves basis set in the interstitial region. Plane wave cut-off of $K_{MAX} = 7.0/R_{MT}$ (R_{MT} is the plane wave radii, and K-max is the maximum modulus for the reciprocal lattice vectors) was chosen for Ag_2O. Values of muffin-tin radii (R_{MT}) are considered to be equal to 1.94 and 1.72 Bohr for Ag and O respectively. In the non-overlapping muffin-tin spheres surrounding the atomic, the spherical harmonics are expanded up to $l_{max} = 10$. The charge density was Fourier expanded up to $G_{max} = 12$ $(Ryd)^{1/2}$. The band structures, electronic and optical calculations are carried out using a number of 1000 k-points in the irreducible Brillouin zone (IBZ). The self consistent calculations are converged since the total energy of the system is stable within 10^{-5} Ry.

3. Results and discussions

3.1. Structural properties

Structural properties of Ag_2O compound are calculated using the volume optimization method. The total energy of Ag_2O is calculated using LDA, GGA and EV–GGA approaches. Volume optimization is performed by minimizing the total energy of the unit cell with respect to the volume of unit cell and total energy was calculated that fitted to the Murnaghan equation of state [21]. It is clear from Fig. 1, that using GGA method, initially energy of unit cell decreases with increase the volume of unit cell, the minimum energy state which is called the ground state energy E_0 of the system is obtained. The volume at the ground state energy E_0, is called the optimum volume or ground state volume of the system. After optimum volume point, the energy then increases with further increase in volume and the system is again in un-relaxed state. Moreover, the variations in lattice constant with the pressure between 0.0 and 20.0 GPa using LDA, GGA and EV–GGA approaches are depicted in Fig. 2. It can be seen from Fig. 2 that the lattice constant decreases with increase the pressure. Also, it is clear from Fig. 1 that using GGA method, the lattice constant ($a_0 = 4.73$ Å) obtained at 0.0 GPa is in good agreement with available experimental data (4.74 Å) [22] and better than that calculated with LDA, EV–GGA and other theoretical results (4.83 Å) [22], (4.81 Å) [23]. As crystal rigidity is measured from Bulk modulus B_0 and thus large value of B_0 is responsible for high crystal rigidity. For Ag_2O, the calculated B_0 is 86.73 GPa greater than 74.0 GPa [23] which show that the Ag_2O is soft semiconductor.

3.2. Elastic properties

The elastic properties define the properties of materials, when it undergo stress, deform and then recover and return to its original shape after stress ceases. These properties play an important role in providing valuable information about binding characteristics between the adjacent atomic plane, structural stability, specific heat, thermal expansion, Debye temperature and many other properties.

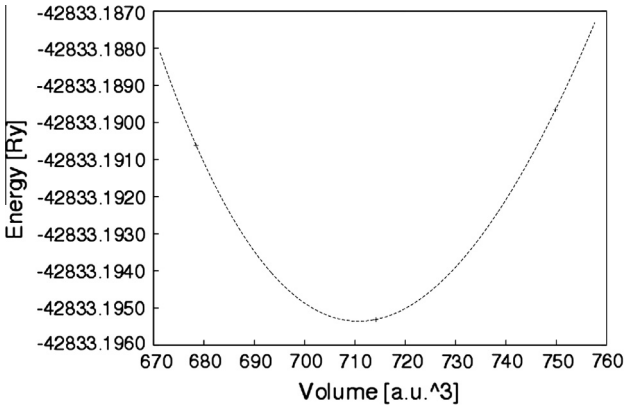

Fig. 1. Volume optimization curve for Ag_2O.

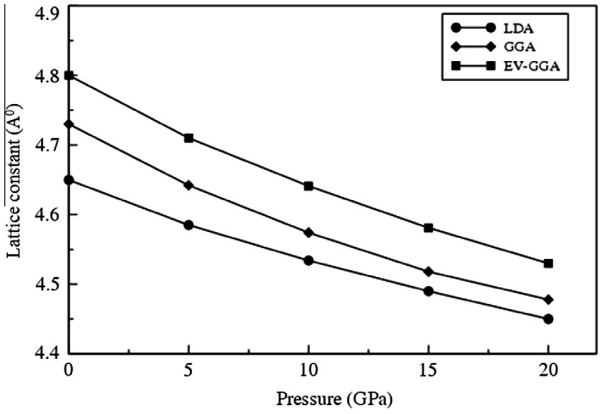

Fig. 2. Lattice constant (Å) verses Pressure (GPa) plot for Ag_2O.

Idea of elastic constants C_{ij} is important to study elastic nature of Ag_2O. Since Ag_2O has cubic symmetry therefore to understand and describe its mechanical behavior, we have calculated only three independent elastic parameters C_{11}, C_{12} and C_{44}. Knowledge of these constants is helpful for information about stability and stiffness of materials. The calculated elastic parameters C_{11}, C_{12} and C_{44} are 132.36, 70.94 and 56.18 GPa respectively. To the best of our knowledge there is no experimental data or theoretical results for the elastic properties of Ag_2O are available in the literature.

It is clear that C_{11}, which is related to the unidirectional compression along the principal crystallographic directions is greater than C_{44}, representing that Ag_2O offer a weaker resistance to the pure shear deformation compared to the resistance and to the unidirectional compression. Following restrictions are imposed on elastic constants in order to have mechanical stability in a cubic structure:

$$\frac{1}{3}(C_{11}+2C_{12})>0; C_{44}>0; \frac{1}{2}(C_{11}-C_{12})>0;\ C_{12}<B<C_{11} \quad (1)$$

Thus Ag_2O is elastically stable as satisfying these restrictions.

The elastic anisotropy (A) has an important implication in industrial science to detect the micro cracks in materials. To detect micro cracks, we have calculated the anisotropy factor (A) by $A = 2C_{44}/(C_{11}-C_{12})$. A material is completely isotropic for $A = 1$ and anisotropic for any value less or greater than unity. As value of anisotropy factor is greater than unity (i.e. $A = 1.829$). Hence, Ag_2O shows anisotropy.

We have applied the Voigt–Reuss–Hill approximation [24] to evaluate the Shear moduli (G) from the elastic constants C_{ij}. For this purpose we have taken the arithmetic mean of the two well-known bounds for monocrystals according to Voigt and Reuss [24–26]. In this way the moduli for the cubic structure are defined as:

$$G_V = \frac{1}{5}(C_{11}-C_{12}+3C_{44}) \quad (2)$$

$$G_R = \frac{5C_{44}(C_{11}-C_{12})}{4C_{44}+(C_{11}-C_{12})} \quad (3)$$

$$B_V = B_R = \frac{(C_{11}+2C_{12})}{3} \quad (4)$$

Thus shear modulus G is written as:

$$G = \frac{(G_V + G_R)}{2} \tag{5}$$

The calculated G_V, G_R and G are 45.992, 42.194 and 44.093 GPa respectively. We have also predicted the Young's modulus (Y), and the Poisson's ratio (v), which is related to the bulk modulus B and the shear modulus G by the following equations.

$$Y = \frac{9BG}{(3B + G)} \tag{6}$$

$$v = \frac{(3B - 2G)}{2(3B + G)} \tag{7}$$

Young's moduli (Y) measure the stiffness of a material. The material shows high stiffness for large value of Y = 113.111 GPa. Poisson's ratio (v) provides information about the bonding forces than any of the other elastic property [25]. The upper and lower limits for central force in solids are 0.5 and 0.25 respectively. Hence, the force is central as Poisson's ratio (v) for Ag_2O is 0.2826.

The ductile or brittle nature of a material is calculated from (B/G) and Poisson's ratio (v). According to Pugh's [26] ratio, higher B/G ratio is responsible for ductile nature while smaller B/G ratio show brittle behavior of the material. The critical number separating ductile from brittle was found to be 1.75. Ductility and brittleness of materials are distinguished in terms of Poisson's ratio (v) and have calculated critical value as 0.26. Materials show brittle nature if Poisson's ratio is less than 0.26 while ductile nature for Poisson's ratio higher than 0.26. Thus, Ag_2O show ductile nature as clear from values of B/G = 1.967 > 1.75 and v = 0.2826.

3.3. Thermal property

Debye temperature (θ_D), representing the effective cutoff frequency of the material was calculated using elastic constants in terms of the following relations [27,28]:

$$\theta_D = \frac{h}{k}\left[\frac{3n}{4\pi}\left(\frac{\rho N_A}{M}\right)\right]^{1/3} V_m \tag{8}$$

where h and k are the Plank's and Boltzmann's constants respectively, n is the number of atoms per formula unit, N_A is the Avogadro's number, ρ is the density of compound, M is the molecular mass per formula unit, and V_m is the average wave velocity [27,29] and is given by:

$$V_m = \left[\frac{1}{3}\left(\frac{2}{V_t^3} + \frac{1}{V_l^3}\right)\right]^{-1/3} \tag{9}$$

where V_l and V_t, are the longitudinal and transverse elastic wave velocities, respectively, which are obtained from Navier's equations [27,29]:

$$V_l = \left(\frac{3B + 4G}{3\rho}\right)^{1/2} \tag{10}$$

$$V_t = \left(\frac{G}{\rho}\right)^{1/2} \tag{11}$$

These calculated Debye temperature, longitudinal, transverse and average elastic wave velocities at zero pressure for Ag_2O are 432 K, 4489.5, 2471.25 and 4332.09 m/s respectively. To the best of our knowledge there is no other theoretical and experimental data exist for comparison.

3.4. Electronic properties

Knowledge about the nature of bonding among different atoms can be explained from charge density distribution of a compound. Transfer of charge between anion and cation can be used to explain ionic character of a material while sharing of charge between the anion and cation is related to the covalent character. We have calculated the charge density of Ag_2O compound at 0.0 GPa in (1 1 0) crystallographic plane, in 3D as displayed in Fig. 3. It is clear from Fig. 3 that the bonding nature between Ag and O is partially covalent and partially ionic and most of the charge density around Ag atom is due to the d orbital while p orbital mainly contributes to the density around Oxygen atom.

3.5. Band structures

We have calculated the electronic band structure for Ag_2O at zero pressure using LDA, GGA EV–GGA and mBJ as shown in Fig. 4. At zero pressure, a narrow and direct band gap occurs for Ag_2O at Γ-symmetry point of the Brillouin zone and the band gap values are found to be 0.155, 0.176, 0.41 and 0.63 eV using LDA, GGA, EV–GGA and mBJ respectively. At 0.0 GPa, the band gap (0.63 eV) obtained with mBJ is in agreement with experimental band gap (1.4 eV) [1] and better than other calculated band gap (0.40 eV) [7]. It is clear from Fig. 5 that while using mBJ plus GGA, an increase in the band gap was observed for Ag_2O at different pressures from 5.0 to 20.0 GPa. Furthermore, the variations in band gap (in eV) of Ag_2O verses pressure (in GPa) is plotted in Fig. 6, clear increases in the band gap with applying pressure between 0.0 and 20.0 GPa is observed. At 20.0 GPa, a slightly large and direct band gap (0.91 eV) is obtained using mBJ and found to be better than that calculated with LDA, GGA and EV–GGA as depicted in Fig. 6.

Density of states (DOS) provides more information about the electronic nature of the material. For Ag_2O, total and partial density of states (DOS) plots at 0.0 GPa and 20.0 GPa pressure are shown in Fig. 7. One can see that at zero pressure, the TDOS below Fermi-level mainly consists of three regions. First region occurs in the energy range from −7.0 eV to −6.3 eV, is dominated by p-state of oxygen atom, while the second region between −4.6 eV and −2.8 eV, is mainly contributed by d-state of Ag. The third region occurring just below the Fermi-level in the energy range from −1.0 eV to 0.0 eV is due to hybridization of Ag–d and O–p states. With increase in pressure from 5.0 GPa to 20.0 GPa, increase in band gap above Fermi-level was observed. At 20.0 GPa, a narrow and direct band gap can be predicted from TDOS of Ag_2O which is comparable to one as depicted in Fig. 5(e).

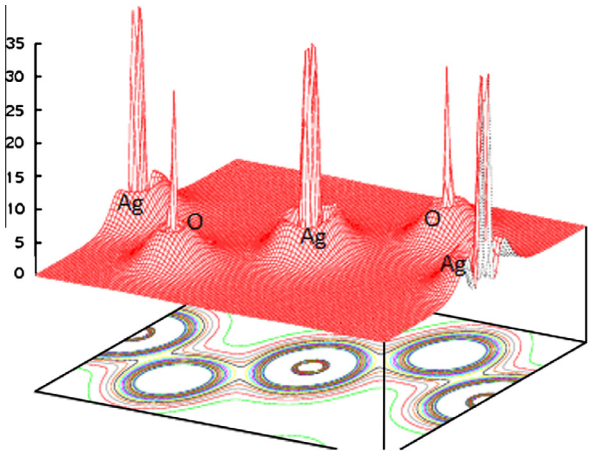

Fig. 3. Electronic charge density of Ag_2O.

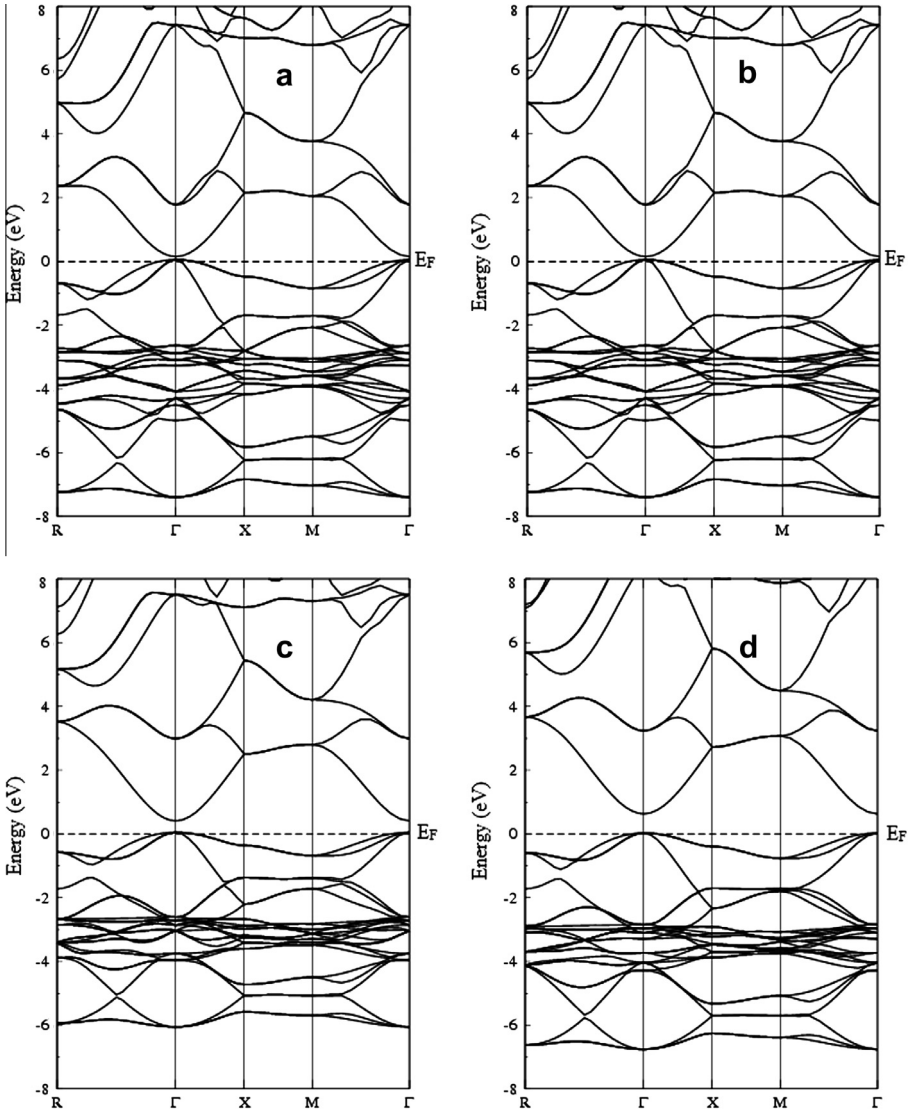

Fig. 4. Electronic band structure of Ag_2O at zero pressure (a) LDA, (b) GGA, (c) EV–GGA and (d) mBJ.

3.6. Optical properties

In this section, we have calculated frequency dependent optical properties such like complex dielectric function, reflectivity and optical conductivity at a pressure between 0.0 and 20.0 GPa using mBJ plus GGA approach. Photons interaction with a material is described by the real and imaginary parts of complex dielectric function. The real and imaginary parts of dielectric function at pressure between 0.0 and 20.0 GPa for Ag_2O is shown in Fig. 8a. Maximum absorption is observed in energy range from 3.65 eV to 5.78 eV at the pressure between 0.0 and 20.0 GPa. It is clear from Fig. 8a that the zero pressure absorption edge starts from small energy and reaches a maximum peak value of $\varepsilon_2(\omega)$ is 8.23 at 4.17 eV. With increase in pressure from 5.0 to 20.0 GPa, variations in peak values of $\varepsilon_2(\omega)$ are found. Maximum peak values are 8.74, 8.95, 8.71 and 8.45 for a pressures of 5.0 GPa, 10.0 GPa, 15.0 GPa and 20.0 GPa respectively. Due to electron transition from top of valence band to lower part of conduction band, absorption threshold occurs at Γ-symmetry point. A material with band gap less than 3.1 eV is very suitable for devices operating in visible region of light. On the other hand, a material with band gap larger than 3.1 eV is best for ultraviolet (UV) purposes [30–34]. Hence, the material is suitable for optoelectronic purposes in the infrared (IR) energy range.

For Ag_2O, variation of real part of dielectric function $\varepsilon_1(\omega)$ for pressures (0.0–20.0 GPa) in energy range from 0.0 to 12.0 eV is also calculated as shown in Fig. 8b. At zero frequency, $\varepsilon_1(0)$ has value of about 4.91 for 0.0 GPa pressure and is found to be increased with increasing the pressure. While at 20.0 GPa, the value of $\varepsilon_1(0)$ reaches up to 5.34. This trend in under pressure study of Ag_2O reveal the inverse behavior of $\varepsilon_1(0)$ with the electronic band gap, which has also been observed for other materials [35,36]. It is clear from Fig. 8b that $\varepsilon_1(\omega)$ increases with increase in energy till reaches to its maximum. At 0.0 GPa, the peak value of $\varepsilon_1(\omega)$ is found to be 9.53 at 3.58 eV and then decreases with increase in energy. It becomes negative at 7.90 eV and then increases at higher energies. Also at high pressure, $\varepsilon_1(\omega)$ decreases after peak value and becomes negative (i.e. light is completely attenuated). Negative values of $\varepsilon_1(\omega)$ occurs at 5.22, 5.32, 5.35 and 5.50 eV for 5 GPa, 10 GPa, 15 GPa and 20 GPa respectively. Frequency dependent reflectivity for Ag_2O at 0.0–20.0 GPa is shown in Fig. 9. The maximum of reflectivity occurs in the energy range from 3.8 to 5.8 eV. At zero pressure, the zero frequency reflectivity $R(0)$ of Ag_2O is 14% and then increases to 16% on increasing pressure to 20 GPa. The highest peaks of the reflectivity are observed at 5.42 eV, 5.48 eV and the smallest at 5.18 eV and 5.53 eV. Pressure encounter broadening of the maximum reflectivity range, is in

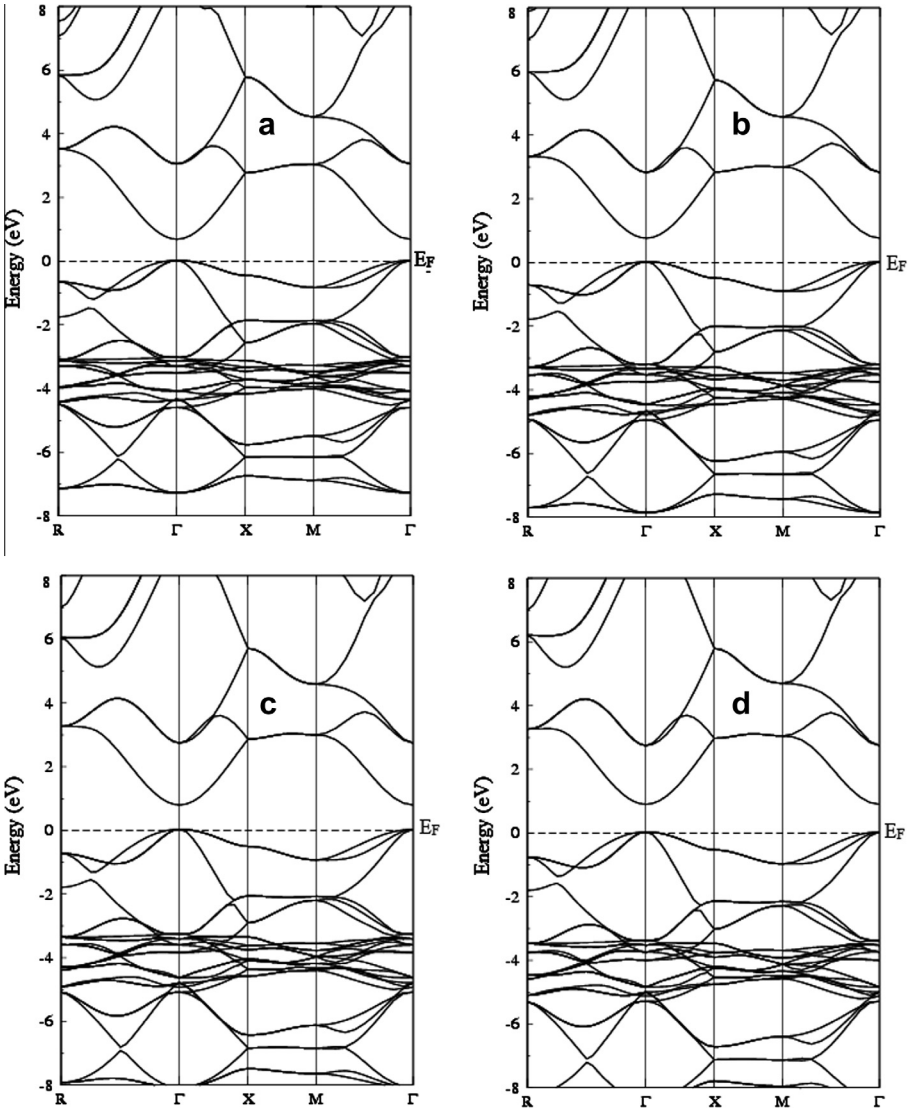

Fig. 5. Electronic band structures of Ag_2O using mBJ at (a) $P = 5$ GPa (b) $P = 10$ GPa (c) $P = 15$ GPa (d) $P = 20$ GPa.

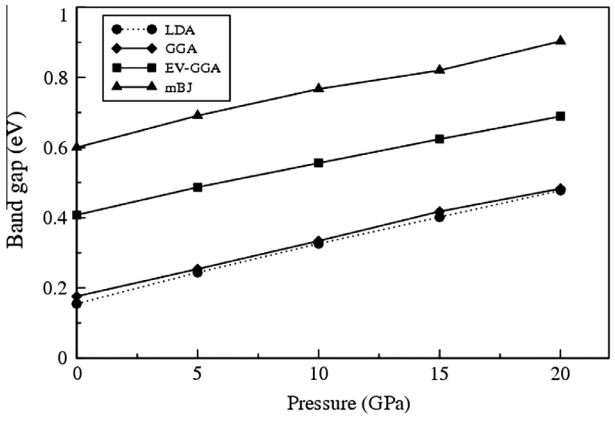

Fig. 6. Band gap (eV) verses pressure (GPa) plot for Ag_2O using mBJ.

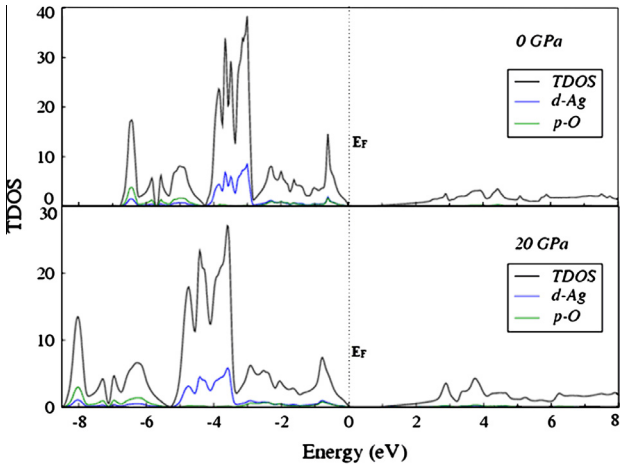

Fig. 7. Total density of states (TDOS) of Ag_2O using mBJ at 0.0 GPa and 20.0 GPa pressure.

accordance to the negative values of real part of dielectric function $\varepsilon_1(\omega)$ [30]. At 0.0 GPa, maximum reflectivity was found to be 36.07% at 5.18 eV which is also in agreement to the maximum negative value of $\varepsilon_1(\omega)$ at 7.95 eV.

The optical conductivity for Ag_2O at pressure between 0.0 and 20.0 GPa in the energy range from 0.0 to 13.0 eV is shown in

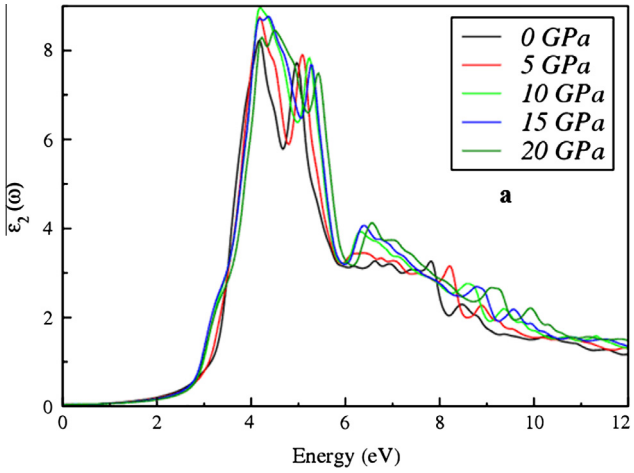

Fig. 8a. Calculated imaginary part of dielectric function of Ag_2O using mBJ at 0.0–20.0 GPa pressure.

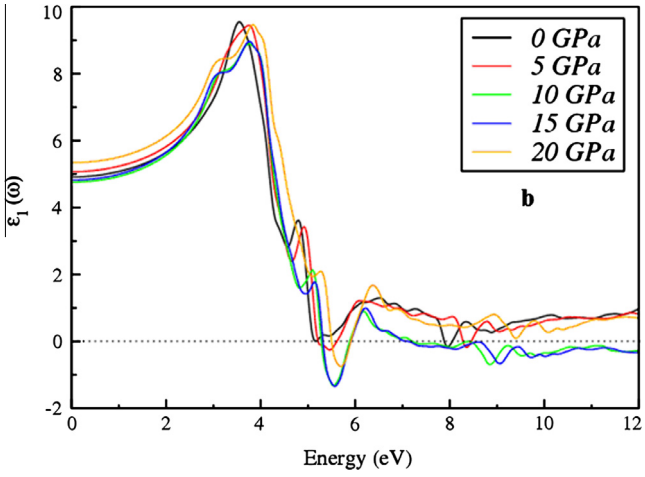

Fig. 8b. Calculated real part of dielectric function of Ag_2O using mBJ at 0.0–20.0 GPa pressure.

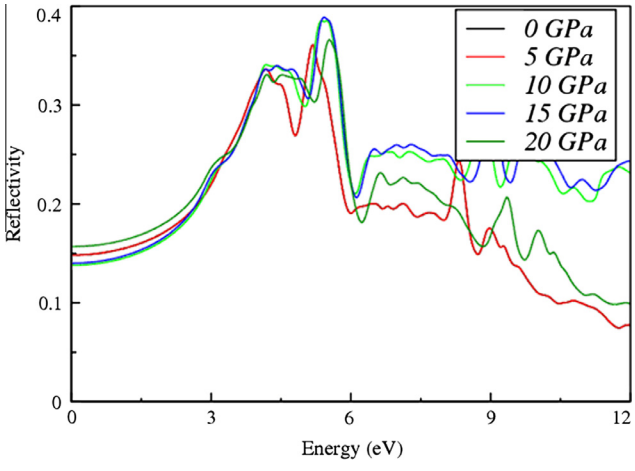

Fig. 9. Calculated frequency dependent reflectivity of Ag_2O using mBJ at 0.0–20.0 GPa pressure.

Fig. 10. Threshold of optical conductivity at zero pressure start from 2.3 eV. After threshold point, the optical conductivity increases and different peaks are observed for 0.0–20.0 GPa pressure.

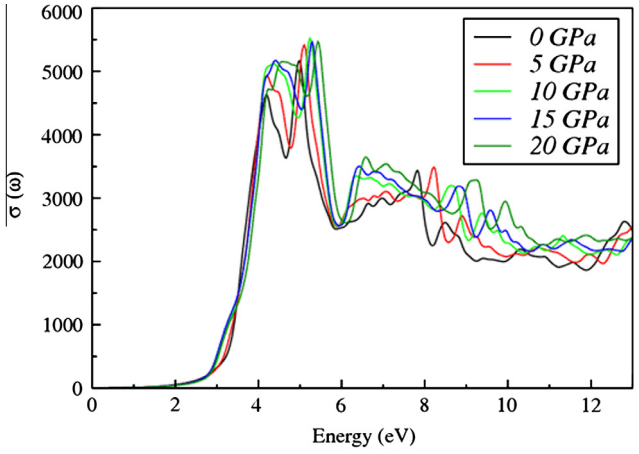

Fig. 10. Calculated optical conductivity of Ag_2O using mBJ at 0.0–20.0 GPa pressure.

Maximum peak values of optical conductivity are 5163.36, 5414.16, 5518.03, 5462.45 and 5468.82 $\Omega^{-1}\,cm^{-1}$ for 0.0 GPa, 5.0 GPa, 10.0 GPa, 15.0 GPa and 20.0 GPa respectively.

4. Conclusions

In this paper, the structural, elastic, thermal, electronic and optical properties of Ag_2O are performed using density functional theory within LDA, GGA, EV–GGA and the modified Becke Johnson potential plus GGA (mBJ–GGA). Using GGA, the calculated structural properties at 0.0 GPa pressure are in good agreement with the available experimental data. To the best of our knowledge there is no experimental data or theoretical results for elastic, thermal and optical properties of Ag_2O, are available in the literature, hence, our calculated results can be serve as a prediction for future investigation. It is concluded that the material is elastically stable, soft semiconductor, ductile and show covalent nature. It is summarized that mBJ presents better band gap values than obtained with LDA, GGA and EV–GGA. Also, a slightly large narrow and direct band gap was found at high pressure using mBJ plus GGA. From optical properties, it is predicted that Ag_2O is suitable for optoelectronic devices. Above 30% of reflectivity occurs in the 3.8–5.8 eV energy. The peak values of optical conductivity are observed above 5000 $\Omega^{-1}\,cm^{-1}$ for 0–20 GPa.

Acknowledgments

The result was developed within the CENTEM project, Reg. No. CZ.1.05/2.1.00/03.0088, co-funded by the ERDF as part of the Ministry of Education, Youth and Sports OP RDI programme.

The author Haleem Ud Din, is highly acknowledges the useful comments and suggestions of Dr. G. Murtaza for this work.

References

[1] K.Z. Yahia, Eng. Tech. 26 (2008) 10.
[2] F.I. Kreeingold, B.S. Kulinkin, Son Phys. Semicond. 4 (1971) 2022.
[3] T.L. Rollins, F.L. Wcichmai, Phys. State Solid 15 (1966) 233–237.
[4] J. Tominaga, J. Phys. Condens. Matter 15 (2003) 25.
[5] Z. Wisniewski, R. Wisniewski, J.L. Nowinski, Solid State Ionics 157 (2003) 275–280.
[6] H. Takahashi, N. Rikitake, T. Sakuma, Y. Ishii, Solid State Ionics 168 (2004) 93–98.
[7] A.B. Gordienko, Y.N. Zhuravlev, D.G. Fedorov, Phys. Solid State 49 (2007) 223–228.
[8] S.a. Beccara, G. Dalba, P. Fornasini, R. Grisenti, A. Sanson, Phys. Rev. Lett. 89 (2002) 025503.
[9] A. Sanson, F. Rocca, G. Dalba, P. Fornasini, R. Grisenti, M. Dapiaggi, G. Artioli, Phys. Rev. B 73 (2006) 214305.
[10] B.J. Kennedy, Y. Kubota, K. Kato, Solid State Commun. 136 (2005) 177–180.
[11] A. Sanson, Solid State Commun. 151 (2011) 1452–1454.

[12] K.S. Pitzer, R.E. Gerkin, L.V. Gregor, C.N.R. Rao, Pure Appl. Chem. 2 (1961) 211–214.
[13] P. Hohenberg, W. Kohn, Phys. Rev. B. 136 (1964) 864.
[14] D.D. Koelling, B.N. Harmon, J. Phys. C: Solid State Phys. 10 (1977) 3107.
[15] P. Blaha, K. Schwarz, G.K.H. Madsen, D.K vasnicka, J. luitz, Wien2k, An Augmented Plane Wave Local orbitals program for calculating crystal properties, Karlheinz Schwarz, Techn. Universitat, Wien, Austria, ISBN 2001, 3-9501031-1-2.
[16] W. Kohn, L.J. Sham, Phys. Rev. A. 140 (1965) 1133.
[17] A.H. Reshak, X. Chen, S. Auluck, H. Kamarudin, Mat. Chem. Phys. 137 (2012) 346–352.
[18] A.H. Reshak, X. Chen, S. Auluck, H. Kamarudin, J. Appl. Phys. 112 (2012) 053526.
[19] A.H. Reshak, I.V. Kityk, O.V. Parasyuk, A.O. Fedorchuk, Z.A. Alahmed, N. Al Zayed, H. Kamarudin, S. Auluck, J. Mater. Sci. 48 (2013) 1342–1350.
[20] A.H. Reshak, I.V. Kityk, O.V. Parasyuk, H. Kamarudin, S. Auluck, J. Phys. Chem. B. 117 (2013) 2545–2553.
[21] F. Birch, J. Geophys. Res. 83 (1978) 1257.
[22] R.G.W. Wyckoff, Crystal Structures, vol. 1, Wiley, New York, 1965.
[23] F. Pei, S. Wu, G. Wang, M. Xu, S.Y. Wang, L.Y. Chen, J. Kor. Phys. Soc. 55 (2009) 1243–1249.
[24] M.J. Mehl, B.M. Barry, D.A. Papaconstantopoulos, in: J.H. Westbrook, R.L. Fleischeir (Eds.), Intermetallic Compounds: Principle and Practice, Principles, vol. I, John Wiley and Sons, London, 1995, pp. 195–210.
[25] B. Mayer, H. Anton, E. Bott, M. Methfessel, J. Sticht, P.C. Schmidt, Intermetallics 11 (2003) 23.
[26] S.F. Pugh, Philos. Mag. 45 (1954) 823.
[27] Z. Sun, S. Li, R. Ahuja, J.M. Schneide, Solid State Commun. 129 (2004) 589.
[28] P. Wachter, M. Filzmoser, J. Rebizant, Physica B 293 (2001) 199.
[29] O.L. Anderson, J. Phys. Chem. Solid 24 (1963) 909.
[30] B. Amin, I. Ahmad, M. Maqbool, J. Lightwave Technol. 28 (2010) 223.
[31] B. Amin, I. Ahmad, M. Maqbool, Appl. Phys. Lett. 26 (2009) 2180.
[32] M. Maqbool, I. Ahmad, H.H. Richardson, M.E. Kordesch, Appl. Phys. Lett. 91 (2007) 193511.
[33] J. Wu, E.E. Haller, H. Lu, W.J. Schaff, Y. Saito, Y. Nanishi, Appl. Phys. Lett. 80 (2002) 3967.
[34] T. Matsuoka, H. Okamoto, M. Nakao, H. Harima, E. Kurimoto, Appl. Phys. Lett. 81 (2002) 1246.
[35] A. Sajid, G. Murtaza, A.H. Reshak, Mod. Phys. Lett. B 27 (2013) 1350061.
[36] G. Murtaza, I. Ahmad, J. Appl. Phys. 111 (2012) 123116.